

Interplay of Carrier Multiplication Pathways in PbSe Nanocrystals and Bulk

Kirill A. Velizhanin and Andrei Piryatinski*

Center for Nonlinear Studies (CNLS), Theoretical Division,
Los Alamos National Laboratory, Los Alamos, NM 87545

(Dated: March 29, 2024)

Using earlier developed exciton scattering model, we report a numerical study of the photogeneration and population relaxation processes contributing to carrier multiplication (CM) in PbSe nanocrystals and bulk. It is found that the photogeneration provides small contribution to the total quantum efficiency compared to the population relaxation process. The resonant incoherent biexciton production is found to be main mechanism of CM in *both* cases of direct biexciton photogeneration and during the population relaxation. Comparison to the published experimental data shows that the calculations reproduce experimentally observed trends providing insight into the mechanisms of CM.

Recent efforts in developing new efficient photovoltaic devices have turned significant attention to the problem of carrier multiplication (CM) in semiconductor materials [1, 2]. Initially reported ultrafast spectroscopic study of nanocrystals (NCs) [3–5] suggested that nanostructuring is a direct way to significantly increase the CM quantum efficiency (QE), i.e. number of electron-hole pairs (excitons) produced per absorbed photon. This assumption was supported by the following arguments: An enhancement of the Coulomb interactions between carriers due to their spatial confinement should lead to more efficient exciton production. A relaxation of the quasimomentum conservation constraint by breaking the translational symmetry should open additional pathways for CM while the intraband cooling is slowed down by the presence of the phonon bottleneck. More recent reports claim much lower QE or the absence of CM in NCs [6–9]. The controversy possibly rise from experimental inaccuracy [8], sample-to-sample variation in surface properties [10], and contribution from extraneous effects such as photocharging [11, 12]. Comparison to the bulk PbS and PbSe spectroscopic measurements shows that bulk QE exceeds validated QE in NCs if compared on the scale of absolute energy [13]. These issues call for the reassessment of the quantum confinement role in the CM dynamics which should be based on unified theoretical model [7].

From theory point of view, multiexciton photogeneration [5, 14], coherent multiexciton production [15, 16], and incoherent impact ionization (II) [17–19], are currently under debate as primary mechanisms of CM. The *ab initio* calculations performed for small ($\lesssim 1$ nm) clusters demonstrated the role of strong Coulomb correlations in photogeneration of multiexcitons and emphasized the role of fast exciton-biexciton dephasing processes [20]. Atomistic calculations focused on *small* diameter ($\lesssim 3$ nm) NCs show that CM is dominated by II processes [19, 21]. Further extrapolation of these calculations to larger NCs and comparison to the bulk have been reported recently [22]. Effective mass models have been used to study direct photogeneration [23] and co-

herent CM dynamics in larger (4–6 nm) diameter NCs. Reported experimental studies consider even larger NCs with the diameter varying up to 10 nm. However, no systematic investigation of *all* CM pathways including photogeneration and population relaxation in various size NCs and comparison to the bulk limit has been reported yet.

In this letter, we report such study for PbSe NCs and bulk. Using earlier developed exciton scattering model accounting for the biexciton photogeneration during interaction with pump and population relaxation processes following the photoexcitation on equal footing [24], we evaluate the contributions of all predicted pathways to the total QE. By introducing the bulk limit as thermodynamic limit, we consider the quantum-confinement induced size-scailing of the quantities of interest. Below, comparison to the bulk limit is reported on absolute energy scale which is relevant to establish direct connection between variation of QE and key quantities such as density of states (DOS) and Coulomb couplings [22]. Performance of photovoltaic devices depends on variously defined energy efficiency [12, 22], which in particular shows up on the energy scale normalized per NC/bulk band gap, E_g [25]. Since, we focus on fundamental mechanisms of CM rather than applications, the latter unitless energy scale is not used below.

We consider an ensemble of NCs in which no more than one photon can be absorbed per NC leading to creation of either exciton or biexciton state. In this case QE can be defined as

$$QE = (2N_{xx} + N_x)/(N_{xx} + N_x), \quad (1)$$

where N_x and N_{xx} are the total non-equilibrium exciton and biexciton populations produced in the ensemble, respectively. They both depend on the delay time measured from the center of the pump pulse and allow one to determine both the QE due to the photogeneration event and the total QE after the population relaxation. For the ensemble of NCs, the bulk limit can be defined as the thermodynamic limit: $V \rightarrow \infty$, $V/v \rightarrow \infty$, and $v = \text{const}$. Here, V is a NC volume, v is the unit cell

volume, and ratio V/v gives number of unit cells in the NC. QE introduced in Eq. (1) is volume independent in the bulk limit, and thus referred to as the *intensive* parameter. As a result, QE scaling with NC size compared to the bulk limiting value provides convenient measure of quantum-size effects. In general, the populations N_x and N_{xx} as well as DOS and Coulomb interactions (determining N_x and N_{xx}) are not intensive parameters. To make proper comparison with the bulk limit, below, we eliminate their volume scaling by multiplying them with powers of (v/V) .

We start by defining the populations n_a^x and n_k^{xx} of a -th exciton and k -th biexciton states, respectively. Their time evolution during the interaction with pump pulse (photogeneration) and further population relaxation are numerically calculated using the weak Coulomb limit of our exciton scattering model. [24] Since in NCs the CM dynamics takes place in the high DOS region, we recast n_a^x and n_k^{xx} to the quasicontinuous frequency representation: $n_x(\omega) = \sum_{a \geq 1} n_a^x \delta(\omega - \omega_a^x)$ and $n_{xx}(\omega) = \sum_{k \geq 1} n_k^{xx} \delta(\omega - \omega_k^{xx})$. Accordingly, the *intensive* populations entering Eq. (1) can be defined as $N_x = (v/V) \int_0^\infty d\omega n_x(\omega)$ and $N_{xx} = (v/V) \int_0^\infty d\omega n_{xx}(\omega)$.

In ultrafast CM experiments, pump duration is usually longer than typical dephasing time leading to the continuous wave (CW) excitation regime. Our numerical calculations show that the contributions of the coherences and interfering sign-varying terms to n_a^x and n_k^{xx} are negligible. As a result, in CW regime the photogenerated biexciton population can be represented as

$$\begin{aligned} N_{xx}(\omega_{pm}) = & \quad (2) \\ & \frac{\mathcal{A}}{\hbar^2} \int d\omega' [V_{eff}^{x,xx}(\omega_{pm}, \omega')]^2 \frac{\tilde{\rho}_x(\omega_{pm}) \rho_{xx}(\omega')}{(\omega' - \omega_{pm})^2 + \gamma^2} \\ & + \frac{\mathcal{A}}{\hbar^2} \int d\omega' [V_{eff}^{x,xx}(\omega', \omega_{pm})]^2 \frac{\tilde{\rho}_x(\omega') \rho_{xx}(\omega_{pm})}{(\omega' - \omega_{pm})^2 + \gamma^2} \\ & + \frac{\mathcal{A}}{\hbar^2} \int d\omega' [V_{eff}^{xx}(\omega')]^2 \frac{\tilde{\rho}_{xx}(\omega' \omega_{pm})}{\omega'^2}, \end{aligned}$$

and the leading contribution to the exciton population as $N_x(\omega_{pm}) = \mathcal{A} \tilde{\rho}_x(\omega_{pm})$. Here, \mathcal{A} is a constant associated with pump fluence, ω_{pm} is the pump frequency, and γ is the dephasing rate between exciton and biexciton states. $\rho_x(\omega) = (v/V)^2 \sum_a \delta(\omega - \omega_a^x)$ and $\rho_{xx}(\omega) = (v/V)^4 \sum_k \delta(\omega - \omega_k^{xx})$ are *intensive* exciton and biexciton DOS, respectively. The associated optically allowed exciton DOS is $\tilde{\rho}_x(\omega) = (v/V) \sum_a |\mu_a^x|^2 \delta(\omega - \omega_a^x)$ and joint biexciton DOS is $\tilde{\rho}_{xx}(\omega_1, \omega_2) = (v/V)^4 \sum_{kl} |\mu_{kl}^{xx}|^2 \delta(\omega_1 - \omega_k^{xx}) \delta(\omega_2 - \omega_l^{xx})$. They depend on vacuum-exciton, μ_a^x , and interband biexciton, μ_{kl}^{xx} , transition dipoles.

Key *intensive* quantity in Eq. (2) is the effective Coulomb interaction which we define as the r.m.s. of the interband Coulomb matrix elements connecting the states with frequencies falling into $[\omega_1, \omega_1 + d\omega_1]$ and

$[\omega_2, \omega_2 + d\omega_2]$ intervals,

$$\begin{aligned} V_{eff}^{x,xx}(\omega_1, \omega_2) = & \left(\frac{V}{v} \right)^2 \left[\sum_{a,m} |V_{a,m}^{x,xx}|^2 \right. \\ & \times \left. \frac{\delta(\omega_1 - \omega_a^x) \delta(\omega_2 - \omega_m^{xx})}{\sum_b \delta(\omega_1 - \omega_b^x) \sum_n \delta(\omega_2 - \omega_n^{xx})} \right]^{1/2}. \end{aligned} \quad (3)$$

Here, ω_a^x (ω_m^{xx}) is a -th exciton (m -th biexciton) state frequency, and $V_{a,m}^{x,xx}$ is the Coulomb matrix element between these states. The size scaling of $V_{eff}^{x,xx}$ in NCs reflects the net result of the Coulomb matrix elements scaling, relaxation of the momentum conservation constraints and the appearance of new selection rules associated with symmetry of the confinement potential. In Eq. (2), $V_{eff}^{x,xx}(\omega)$ denotes effective Coulomb coupling between the vacuum and biexciton manifold.

Three terms in the r.h.s. of Eq. (2) describe the following photogeneration pathways [24]: In the first term the exciton DOS, $\tilde{\rho}_x(\omega_{pm})$, depends on the pump frequency indicating resonant production of single excitons which further scatter to the biexciton manifold. This is the *indirect* biexciton photogeneration pathway predicted by the exciton scattering model [24]. The second term contains biexciton DOS, $\rho_{xx}(\omega_{pm})$, depending on the pump frequency indicating the *direct* biexciton photogeneration through virtual exciton states. Finally, the last term describes the pathway involving direct biexciton generation by optical stabilization of the scattering processes between the vacuum and biexciton manifold. The last two pathways have been first considered in Refs. [5] and [14], respectively.

The population relaxation dynamics is described by a set of kinetic equations introduced in Ref. [24] and further transformed to the quasicontinuous frequency representation. They contain II and Auger recombination rates

$$k_{II}(\omega) = \frac{2\pi}{\hbar^2} [V_{eff}^{x,xx}(\omega)]^2 \rho_{xx}(\omega), \quad (4)$$

$$k_{AR}(\omega) = \frac{2\pi}{\hbar^2} \left(\frac{v}{V} \right)^2 [V_{eff}^{x,xx}(\omega)]^2 \rho_x(\omega), \quad (5)$$

respectively, with $V_{eff}^{x,xx}(\omega) \equiv V_{eff}^{x,xx}(\omega, \omega)$. According to Eq. (4), the II rate depends on intensive parameters and therefore has finite value in the bulk limit. In contrast, the Auger rate has uncompensated volume prefactor and scales to zero as V^{-2} in the bulk limit. The intraband cooling rates also entering the kinetic equations are calculated using Ohmic spectral density under assumption of no phonon bottleneck present in NCs. The total QE is evaluated through numerical solution of the kinetic equations with photogenerated populations used as initial conditions.

To calculate the electron and hole wavefunctions in spherically symmetric PbSe NCs and bulk, we adopted the effective mass formalism due to Kang and Wise [26].

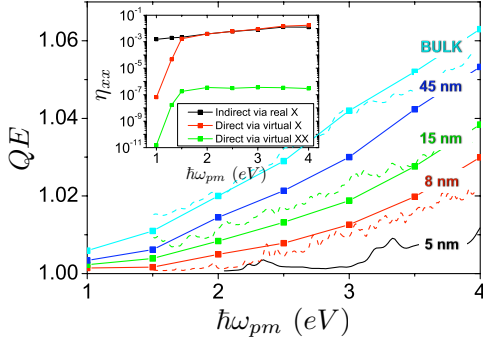


FIG. 1: Photogeneration QE as a function of pump energy for PbSe NCs of diameter $d = 5, 8, 15, 45$ nm and bulk. Solid lines mark QE calculated using general expressions for populations from Ref. [24]. Dash marks approximate results for $d=8, 15$ nm NCs and bulk due to Eq. (6). The inset shows biexciton quantum yield, $\eta_{xx} = QE - 1$, associated with each photogeneration pathway for PbSe NC of $d = 15$ nm.

The exciton and biexciton wavefunctions are introduced as uncorrelated configurations of the electron and hole wavefunctions to evaluate the transition dipoles and the interband Coulomb matrix elements. The exciton (biexciton) dephasing rate is set to 50 meV (100 meV) [20]. To account for degeneracy of the exciton (biexciton) states associated with four equivalent L -valleys, the exciton (biexciton) populations were multiplied by factor 4 (16). The intraband cooling rates were obtained by fitting total intraband relaxation time, τ_{ph} , to reproduce the experimentally observed values in the range $0.5 < \tau_{ph} < 5.0$ ps [13, 19]. The Monte Carlo sampling has been used to handle large size NCs and to average over the Gaussian size distribution with 5% standard deviation.

Calculated photogeneration QE as a function of the pump energy in PbSe NCs and bulk is plotted in Fig. 1. It shows monotonic increase to the bulk values as the diameter of the NC increases. The inset provides contributions of three photogeneration pathways associated with Eq. (2) to the biexciton quantum yield, $\eta_{xx} = QE - 1$. According to Fig. 1, the contribution of the last pathway (green line) is negligible. The other two become equal above the photogeneration energy threshold, ~ 1.5 eV. Taking into account resonant nature of the denominator in the first two terms of Eq. (2), the integral convolutions can be calculated. This results in exactly identical contributions of the first two terms to the biexciton population as observed in Fig. 1, and the latter quantity acquires the following simple dependence on II rate, k_{II} , photogenerated exciton population, N_x , and effective dephasing rate, γ_{eff} , between exciton and biexciton states

$$N_{xx}(\omega_{pm}) = k_{II}(\omega_{pm})N_x(\omega_{pm})/\gamma_{eff}. \quad (6)$$

As a result, the photogeneration QE becomes dependent

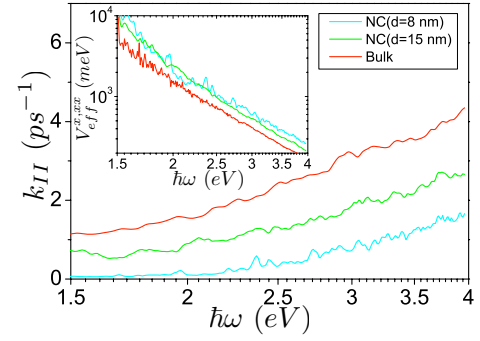


FIG. 2: Calculated II rate as a function of energy for PbSe NCs of diameter $d = 8, 15$ nm and bulk. The inset shows log-log plot of the effective Coulomb interaction.

only on the II rate and effective dephasing rate, $QE = 1 + k_{II}/\gamma_{eff}$. To check this relation, we calculated QE using II rate evaluated according to Eq. (4) (Fig. 2), and $\hbar\gamma_{eff} = 50$ meV. This QE shown by dash in Fig. 1, well reproduce the trends of the “exact” calculations (solid lines).

The analysis above leads to an important conclusion that in the absence of interference destroyed by high DOS and the interband dephasing processes, the photogeneration becomes resonant incoherent process. Approximate Eq. (6) further suggests that the biexciton generation is a *single II event* of the photoexcited exciton states taking place on the dephasing timescale, γ_{eff}^{-1} . Previous studies of photogeneration processes [5, 14], implicitly assumed *constructive* interference *within* the second and the third pathways. This assumption led to the squared (in contrast to our linear) contributions of the exciton and biexciton DOS to the second and the third terms in Eq. (2), respectively, leading to significant overestimation of their contributions. Established linear dependence between the photogenerated QE and II rate (Fig. 2) helps to explain the QE variation with NC size observed in Fig. 1. According to the inset to Fig. 2, the effective Coulomb interaction calculated according to Eq. (3) and entering II rate (Eq. (4)) is enhanced in NCs compared to the bulk limit just by a factor of two. In contrast, the calculations show that the biexciton DOS in NCs is significantly reduced due to quantum-confinement fully overplaying the effective Coulomb enhancement. The dominant role of the DOS in II rate explains the monotonic increase of QE in NC with their size as observed in Fig. 1.

In contrast to II rate (Eq. (4)), the volume scaling of Auger recombination rate (Eq. (5)) makes this competing process negligible in the region of high DOS. Therefore, the QE associated with the population relaxation process is fully determined by the interplay between II and cooling time, τ_{ph} , which in our case are comparable. Fig. 3 presents calculated total QE due to both photogeneration and population relaxation processes in PbSe NCs and the

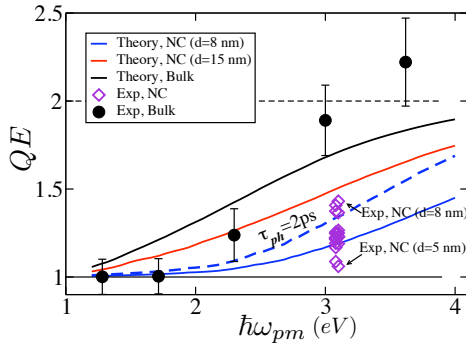


FIG. 3: Total QE as a function of pump energy calculated for PbSe NCs of diameter $d = 8, 15$ nm and bulk. Solid (dash) lines present calculations with $\tau_{ph} = 1$ ps ($\tau_{ph} = 2$ ps). For comparison, diamonds and dots mark experimental data from Refs. [11] and [13], respectively.

bulk. Due to the established size scaling of II rate (Fig 2), the total QE in NCs does not exceed the bulk values. For comparison, the experimental data for PbSe NCs [11] and the bulk [13] are also shown in the plot. Solid lines in Fig. 3, show QE calculated for the intraband cooling time $\tau_{ph} = 1.0$ ps which provides the best fit for the bulk. In general, the theory reproduces the experimental trends in bulk. [28] To get better agreement with experiment for NC of $d = 8$ nm, we had to increase the cooling time up to $\tau_{ph} = 2$ ps (blue dash). The increase of τ_{ph} can be attributed to the quantum confinement induced increase in the level spacing [27]. The photogeneration contribution (Fig. 1) to the total QE (Fig. 3) is small ($\sim 5\%$). This follows from the fact that the photogeneration is a single II event occurring on short ($\lesssim 100$ fs) dephasing timescale. In contrast, during the population relaxation multiple II events take place on much longer ($\gtrsim 1$ ps) timescale and provide major contribution to QE.

To conclude, using the exciton scattering model parameterized by the effective mass Hamiltonian, we have systematically studied the photogeneration and population relaxation pathways contributing to CM in PbSe NCs and bulk. We found that II is the main mechanism of CM during *both* processes which explains weak contribution of the photogeneration to the total QE. We have also found that QE in NCs plotted on *absolute* energy scale does not exceed limiting value in the bulk. This follows from the quantum-confinement induced weak enhancement of the *effective* Coulomb interaction and stronger reduction in the biexciton DOS. Comparison with experiment shows that the theory reproduces observed trends. Our conclusions are valid for the NCs of relatively large ($d \gtrsim 5$ nm) size and bulk where the effective mass approximation works. Smaller NCs should be studied by using the atomistic calculations. Finally, we note that the performance of photovoltaic devices depends on the band gap scaling, and even for the case

of weak Coulomb enhancement, the NCs are potentially good candidates for such applications. Increase in the effective Coulomb interaction and biexciton DOS through the nanoscale heterostructuring and surface functionalization will only improve their potential performance.

This work was supported by the Office of Basic Energy Sciences, US Department of Energy, and Los Alamos LDRD funds. We wish to thank Victor Klimov, Gary Doolen, and Darryl Smith for stimulating discussions and comments on the manuscript.

* Electronic address: apiryat@lanl.gov

- [1] S. Kolodinski, J. Werner, T. Wittchen, and H. Queisser, *Appl. Phys. Lett.* **63**, 2405 (1993).
- [2] A. J. Nozik, *Physica E* **14**, 115 (2002).
- [3] R. D. Schaller and V. I. Klimov, *Phys. Rev. Lett.* **92**, 186601 (2004).
- [4] R. J. Ellingson *et al.*, *Nano Lett.* **5**, 865 (2005).
- [5] R. D. Schaller, V. M. Agranovich, and V. I. Klimov, *Nature Phys.* **1**, 189 (2005).
- [6] G. Nair and M. G. Bawendi, *Phys. Rev. B* **76**, 081304(R) (2007).
- [7] G. Nair, S. M. Geyer, L.-Y. Chang, and M. G. Bawendi, *Phys. Rev. B* **78**, 125325 (2008).
- [8] M. Ben-Lulu *et al.*, *Nano Lett.* **8**, 1207 (2008).
- [9] J. J. H. Pijpers *et al.*, *J. Phys. Chem. C* **112**, 4783 (2008).
- [10] M. C. Beard *et al.*, *Nano Lett.* **9**, 836 (2009).
- [11] J. A. McGuire *et al.*, *Acc. Chem. Res.* **41**, 1810 (2008).
- [12] J. A. McGuire *et al.*, *Nano Lett.* **10**, 2049 (2010).
- [13] J. J. H. Pijpers *et al.*, *Nature Phys.* **5**, 811 (2009).
- [14] V. I. Rupasov and V. I. Klimov, *Phys. Rev. B* **76**, 125321 (2007).
- [15] A. Shabaev, A. L. Efros, and A. J. Nozik, *Nano Lett.* **6**, 2856 (2006).
- [16] W. M. Witzel, A. Shabaev, C. S. Hellberg, V. L. Jacobs, and A. L. Efros, *Phys. Rev. Lett.* **105**, 137401 (2010).
- [17] A. Franceschetti, J. M. An, and A. Zunger, *Nano Lett.* **6**, 2191 (2006).
- [18] E. Rabani and R. Baer, *Nano Lett.* **8**, 4488 (2008).
- [19] G. Allan and C. Delerue, *Phys. Rev. B* **77**, 125340 (2008).
- [20] O. V. Prezhdo, *Acc. Chem. Res.* **42**, 2005 (2009).
- [21] E. Rabani and R. Baer, *Chem. Phys. Lett.* **496**, 227 (2010).
- [22] C. Delerue, G. Allan, J. J. H. Pijpers, and M. Bonn, *Phys. Rev. B* **81**, 125306 (2010).
- [23] L. Silvestri and V. M. Agranovich, *Phys. Rev. B* **81**, 205302 (2010).
- [24] A. Piryatinski and K. A. Velizhanin, *J. Chem. Phys.* **133**, 084508 (2010).
- [25] M. C. Beard *et al.*, *Nano Lett.* **10**, 3019 (2010).
- [26] I. Kang and F. W. Wise, *J. Opt. Soc. Am. B* **14**, 1632 (1997).
- [27] C. Bonati *et al.*, *Phys. Rev. B* **76**, 033304 (2007).
- [28] Observed discrepancy at $1.5 < \hbar\omega_{pm} < 3$ eV are due to the phenomenological nature of the electron-phonon interaction model. For $3 < \hbar\omega_{pm}$ eV, three-exciton generation processes should be added to the theory.